



Application of Recycled Rubber Mats for Improved Performance of Ballasted Tracks

Trung Ngo¹ (✉), Buddhima Indraratna², and Cholachat Rujikiatkamjorn¹

¹ Transport Research Center, School of Civil and Environmental Engineering, University of Technology Sydney, 15 Broadway, Ultimo, NSW 2007, Australia
Trung.Ngo@uts.edu.au

² Civil Engineering and Director, Transport Research Centre, School of Civil and Environmental Engineering, University of Technology Sydney (UTS), 15 Broadway, Ultimo, NSW 2007, Australia

Abstract. This paper summaries the results of a study on the use of recycled rubber mats for improved performance of ballasted tracks. One solution used to minimise ballast degradation (breakage) is to use an innovative recycled rubber mat, known as rubber-energy-absorbing drainage mat (READ), manufactured from end-of-life tires to provide a cost-effective solution to conventional tracks. When placed underneath the ballast, the energy-absorbing nature of the rubber mats decreases the load that is transferred to the ballast, so the ballast experiences less deformation and breakage. In this study, a series of large-scale triaxial tests are conducted to investigate the performance of the READS in the attenuation of cyclic and dynamic loads and subsequent reducing of ballast degradation. Numerical modelling using the Discrete Element Method (DEM) is conducted to investigate the improved performance of ballast in a micromechanical perspective. Evolutions of contact forces and contour stress distributions during cyclic tests are investigated through coupled DEM-FEM model.

Keywords: Recycled rubber mat · Transport geotechnics · Ballast · Breakage · Discrete Element Method (DEM)

1 Introduction

Australian rail sector must continuously upgrade its track network and adopt innovative technology to reduce the cost as well as increased passenger comfort. Ballast layer plays a crucial role in transmitting the train loading to underlying track-formation layers at a reduced stress level [1]. The ballast grains experience significant degradation and breakage when subject to heavy hauls freight trains and moving. Due to ballast breakage, Australian rail industry spends a significant budget in terms of track maintenance, together with improving the ground before track construction where soft and saturated subgrade soils induce considerable difficulties in design and construction [2].

The degradation of ballast aggregates (breakage) significantly influences the shear strength of ballast. Sun et al. [3] conducted large-scale tests on ballast and found that

confining pressure (i.e., lateral confinement) and frequency have a significant influence on the breakage of ballast under cyclic loading. Leng *et al.* [4] conducted cyclic tests on coarse-granular aggregates and the test results showed that there were two separate deformation stages of a rapid increase in deformation initially followed by a steady-state of plastic strain after a given loading cycle. These findings were in agreement with previous literature [5–8], among others. Previous studies found that particle breakage could happen even at small-stress level [9, 10]. In addition, previous studies indicated that increased lateral confinement for ballast resulted in decreased peak friction angles [11].

Research on the application of elastic inclusions (geosynthetics, geocell) for improved performance of tracks and subsequently decreased ballast breakage has been well documented [12–18], among others. Field trials carried out on fully instrumented tracks at Singleton, NSW Australia proved that rubber mat could reduce ballast deformation apart from reduced breakage [19, 20].

There is a lack of study on the use of recycled rubber mats for reducing the breakage of ballast grains from a micro-mechanical perspective. This paper reports the main findings of the study on the use of large-scale triaxial tests and discrete element modelling (DEM) on the breakage responses of railway ballast.

2 Large-Scale Triaxial Cyclic Tests

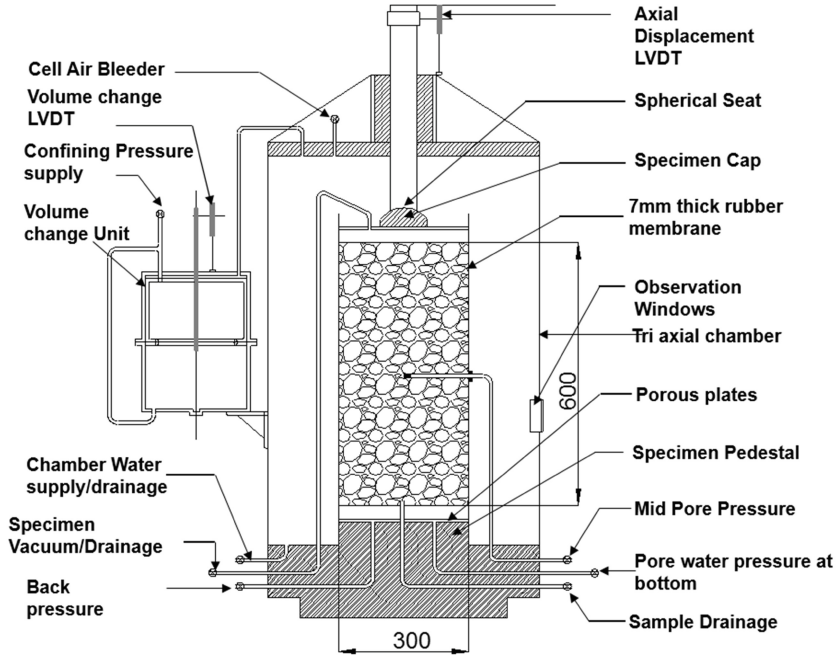
A large-scale triaxial testing apparatus designed and built at the University of Wollongong can accommodate a testing sample of 300 mm diameter and 600 mm high, as detailed in Fig. 1a. Materials tested in the laboratory including ballast, capping materials and recycled rubber mat as shown in Figs. 1b–c. The ballast was cleaned and then passed through a set of standard sieves (53–9.5 mm) followed the Australian Standards (AS2758.7–2015) [21]. Upon drying, the ballast grains were coloured to help in quantifying the amount of breakage after each test. A mixture of sandy soil was adopted for a subgrade layer while a mixture of sand and crushed-rock was adopted for capping.

2.1 Sample Preparation and Testing Procedure

A tested sample was filled by a 200 mm thick subgrade at the bottom and compacted to a density of $\rho = 18.5 \text{ kN/m}^3$. A 100 mm-thick capping was then compacted to $\rho = 20.5 \text{ kN/m}^3$. A layer of rubber mats was then put on top of the capping. A ballast layer (300 mm thick) was placed and compacted to a $\rho = 15.5 \text{ kN/m}^3$. After preparing the specimen, it was filled with water and left overnight to saturate the specimen. Cyclic tests were started under $q_{cyclic-max} = 230 \text{ kPa}$, $q_{cyclic-min} = 30 \text{ kPa}$, frequencies: $f = 10\text{--}40 \text{ Hz}$ and a constant confining pressure of $\sigma_3 = 20 \text{ kPa}$. All tests were sheared up to $N = 500,000$ cycles. During these tests, the permanent vertical displacement, ε_a and volumetric strain, ε_v were measured. Ballast aggregates were recovered after each test, then sieved, and the changes in size distributions were recorded to investigate the amount of breakage.

Measured test data showed that the recycled rubber mats decreased deformation and breakage of ballast. This was because the mat could absorb cyclic and impact loads

(i.e. energy) that led to less energy was transferred to ballast aggregates and thereby decreased breakage. The inclusion of rubber mat reduced the breakage up to 30.8% and 35.3% when subjected to frequencies of $f = 10, 20$ Hz, respectively. Detailed of test results were reported earlier by Indraratna *et al.* [22] and some of the test data were re-used in this study for the calibration of the DEM model.



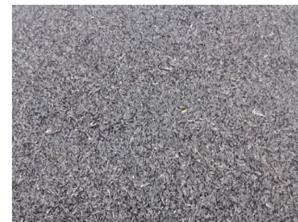
(a)



(b)



(c)



(d)

Fig. 1. (a) a schematic section of triaxial apparatus; (b) mixed ballast in different colours following the gradation; (c) capping aggregates; and (d) recycled rubber mat (READS)

3 Discrete Element Modeling

A discrete element method (DEM) has been widely used to study micro-mechanical responses of granular aggregates [23–28], among others. It is well documented that due to excessive computational time required to carry out cyclic tests in DEM, most of the previous DEM simulations were initiated to only a few thousand loading cycles. Given the excessively computational cost of simulating an actual track embankment in DEM having different layers of track substructure (i.e., ballast, capping, subgrade), thereby a coupled discrete-continuum modelling approach that utilises advantages of both numerical schemes with acceptable computational effort and accuracy is introduced in this study.

3.1 Coupled DEM-FEM

Ballast with varied geometries and sizes were digitalised in DEM by bonding many cylindrical together via parallel bond (Fig. 2a). The breaking (disconnection) of those bonds was approximately considered to represent particle breakage. Micro-mechanical parameters adopted for the DEM analysis were selected by calibration with laboratory test data as presented in Table 1. Figure 2b shows a schematic diagram of a coupled DEM-FEM model for the large-scale triaxial test, where the subgrade, capping and rubber mat was simulated by the continuum method. The schematic diagram of exchanging of forces (F_n , F_s) and displacement ($\dot{X}_i^{[E]}$) between a discrete grain and continuum element at its interface is presented in Figs. 2c-d.

Contact forces at their interface can be calculated as:

$$F_i^{[c]} = F_n^{[c]} + F_s^{[c]} \quad (1)$$

where, normal force ($F_n^{[c]}$) and shear force increment ($\Delta F_s^{[C]}$) can be computed by:

$$F_n^{[C]} = K^n U^n n_i; \quad \text{and} \quad \Delta F_s^{[C]} = -K^s (\Delta X_i^{[C]} - \Delta X_i^{[C]} n_i) \quad (2)$$

Forces and moments on discrete particles can be determined by:

$$F_i^{[P]} \leftarrow F_i^{[P]} - F_i^{[C]}; \quad \text{and} \quad M_i^{[P]} \leftarrow M_i^{[P]} - e_{ijk} (X_j^{[C]} - X_j^{[P]}) F_k^{[C]} \quad (3)$$

Relative velocity (displacement) at the interface (V_i) is given by:

$$V_i = \dot{X}_{i,E}^{[C]} - \dot{X}_{i,E}^{[P]} = \dot{X}_{i,E}^C - \left[\dot{X}_i^{[P]} + e_{ijk} \omega_j^{[P]} (X_k^{[C]} - X_k^{[P]}) \right] \quad (4)$$

where, $\dot{X}_{i,E}^{[C]}$ and $\dot{X}_{i,E}^{[P]}$ are the velocities of elements and discrete grains. $\dot{X}_i^{[P]}$ and $\omega_j^{[P]}$ are the translation and rotation of a grain, and e_{ijk} is the permutation symbol.

The velocity of continuum elements at the interface is then calculated as:

$$\dot{X}_{i,E}^{[C]} = \sum N_j \dot{X}_{i,E}^j \quad (5)$$

where, N_j is a shape function, determined by: $N_j = (1 + \xi_o)(1 + \eta_o)/4, j = 1, 2, 3, 4$; and $\xi_o = \xi_i \xi, \eta_o = \eta_i \eta$; ξ_i and η_i are coordinates of nodes. Shear and normal forces are distributed to the nodal force, $F_i^{[E,j]}$ via shape function N_j :

$$F_i^{[E,j]} = F_i^{[E]} + F_i^{[C]} N_j \tag{6}$$

During load application, contact forces DEM domain (Zone 1) is transferred to continuum domain (Zone 2); and the displacements of continuum elements, are transferred back to the DEM – Zone 1 as boundary conditions. More detail on the model calibration, application of loading and boundary conditions, and laboratory test results can be found in [22].

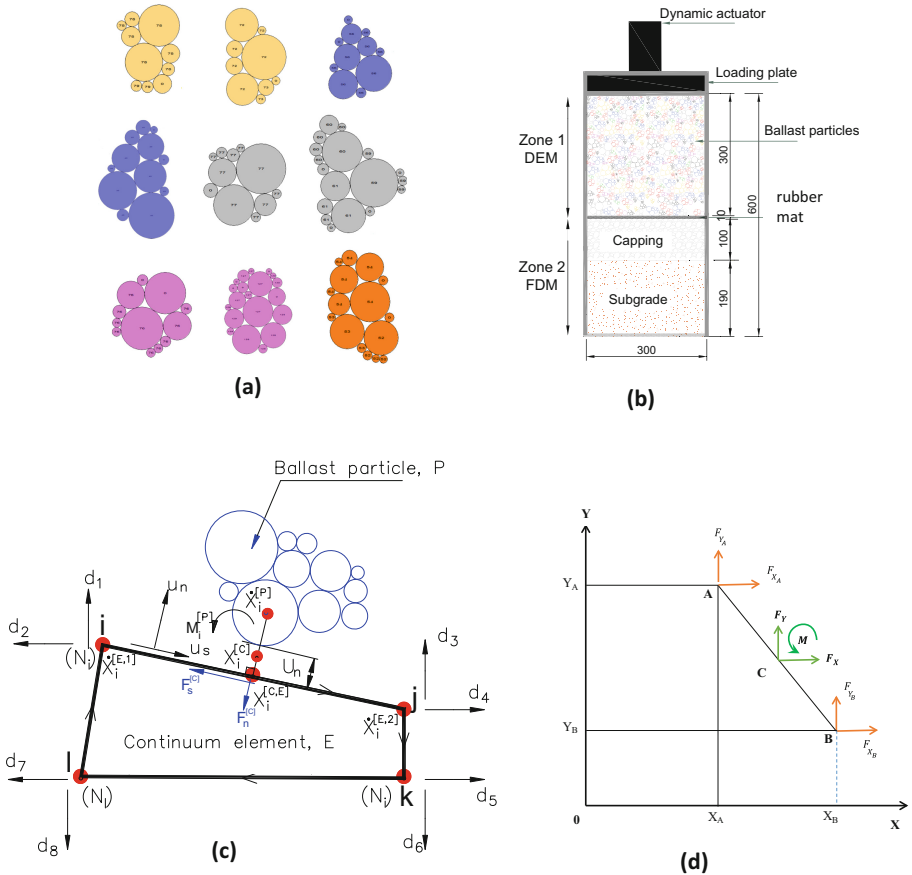


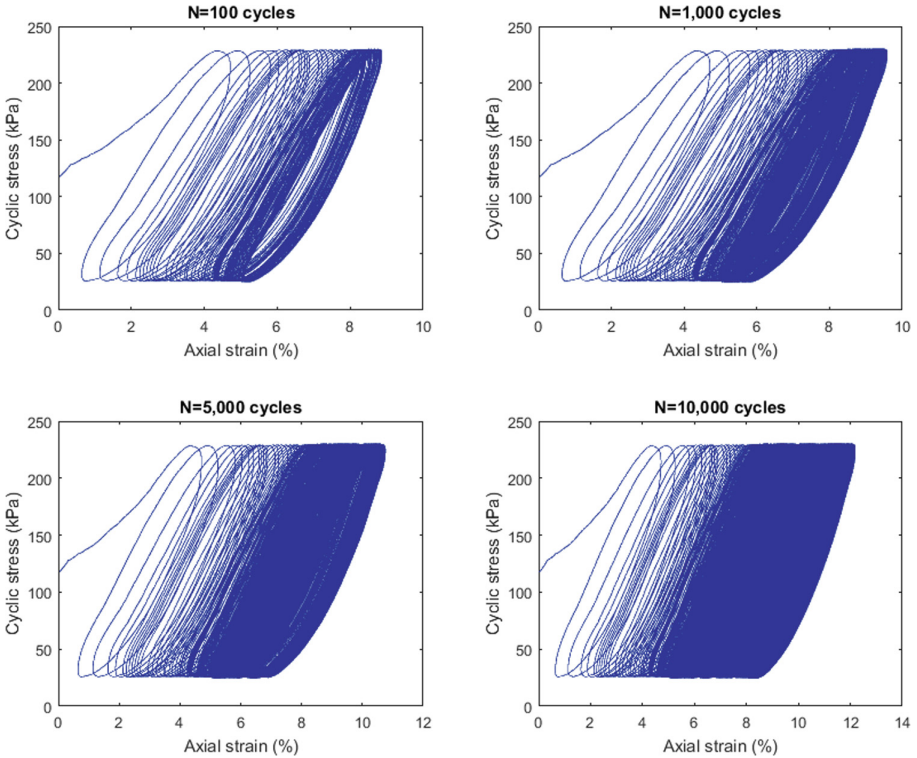
Fig. 2. (a) Simulated ballast grains; (b) coupled DEM-FEM model; and (c) interaction of a grain and an element; and (d) force and moment exchanges (*modified after* [24])

Table 1. Micro-mechanical parameters adopted for DEM analysis

Parameter	Value
Particle density (kg/m^3)	2500
Friction coefficient	0.82
Contact normal stiffness (N/m)	2.52×10^8
Contact shear stiffness (N/m)	1.26×10^8
Contact normal stiffness of wall (N/m)	1.25×10^8
Shear stiffness of wall (N/m)	0.625×10^8
Parallel bond stiffness (N/m)	6.84×10^{10}
Parallel bond shear strength (N/m^2)	486×10^4
Parallel bond radius multiplier	0.50

3.2 Predicted Stress-Strain Behaviour of Ballast

Figure 3 presents predicted cyclic stress-strain from the coupled DEM-FEM model at varied load cycles N subjected to a frequency, $f = 20$ Hz. The predicted strains remarkably increase up to about 5.5% at the first $N = 1000$ load cycles, followed by

**Fig. 3.** Applied cyclic stress versus axial strain ε_a at varying load cycle, N

slightly increased strains up to $N = 5,000$ cycles. After this cycle, the ballast remains relatively unchanged to the end of the simulation ($N = 10,000$ cycles). This indicated that ballast aggregates exhibited remarkable compression and re-arrangement during the initial stage of loading, but after achieving a threshold compression, any subsequently applied loads would resist further deformation and instead, accelerate ballast breakage.

3.3 Simulated Ballast Breakage

The accumulation of bond breaking with increased N subjected to 4 frequencies of $f = 10\text{--}40$ Hz is presented in Fig. 4. It is noted that the breaking of bonds (B_r) within a simulated particle was considered to represent particle breakage. It is worth mentioning that B_r is different from the actual ballast breakage measure in the laboratory, the B_r could supply an indication of the extent of breakage occurs. From DEM-FEM simulation, the B_r increases with an increase in load frequency, f and this trend are similar to the ballast breakage measured in the laboratory data. Subjected to a given f , the number of broken bonds increases significantly within the first $N = 5,000$ cycles; and then keeps

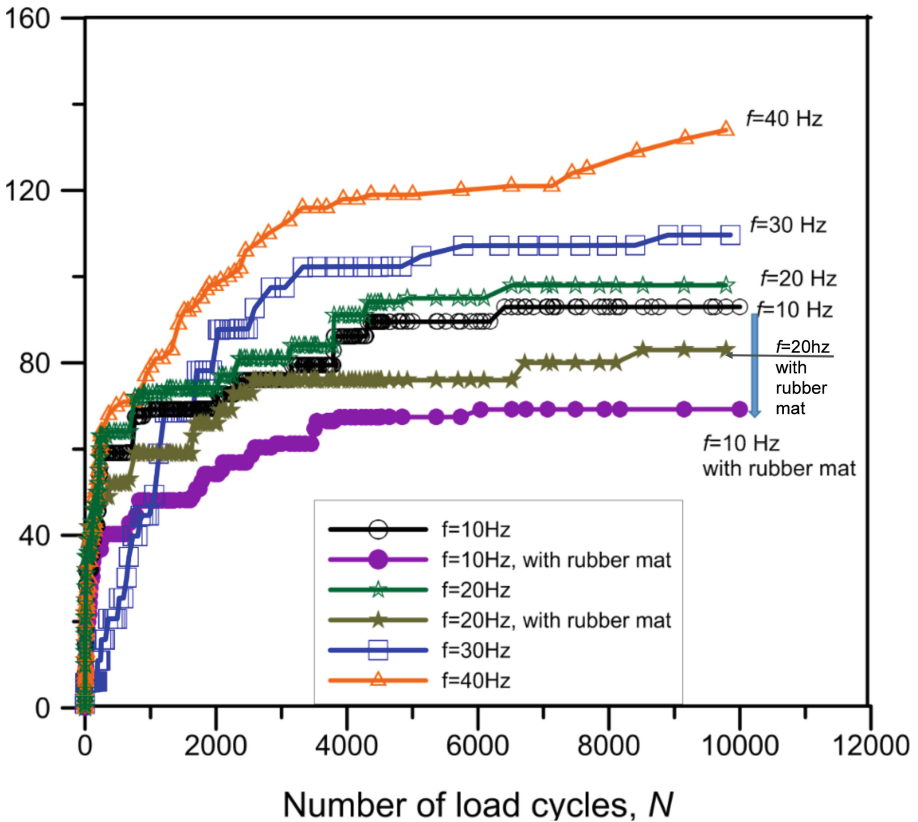


Fig. 4. Predicted contact bond breaking at different frequencies, $f = 10\text{--}40$ Hz with and without recycled rubber mat (adopted from Indraratna et al. 2020 – with permission from ASCE).

almost unchanged at subsequent loading cycles. The inclusion of a recycled rubber mat underneath the ballast layer leads to a decreased B_r ; and this could be attributed to the energy-absorbing characteristics of the rubber mat.

3.4 Contact Force Distributions

Figure 5 presents the distributions of contact forces in the ballast layer and vertical stresses predicted for capping and subgrade layers. Vertical stress contours in the capping and subgrade layers at different load cycles N are also presented where the contour was captured under $f = 20$ Hz. It is seen that the applied cyclic loads are distributed to particles through contact force chains where each contact force is represented at the contact point having a thickness proportional to the force magnitude. Upon cyclic loading, large contact forces appeared and concentrated beneath a top-loading plate. It

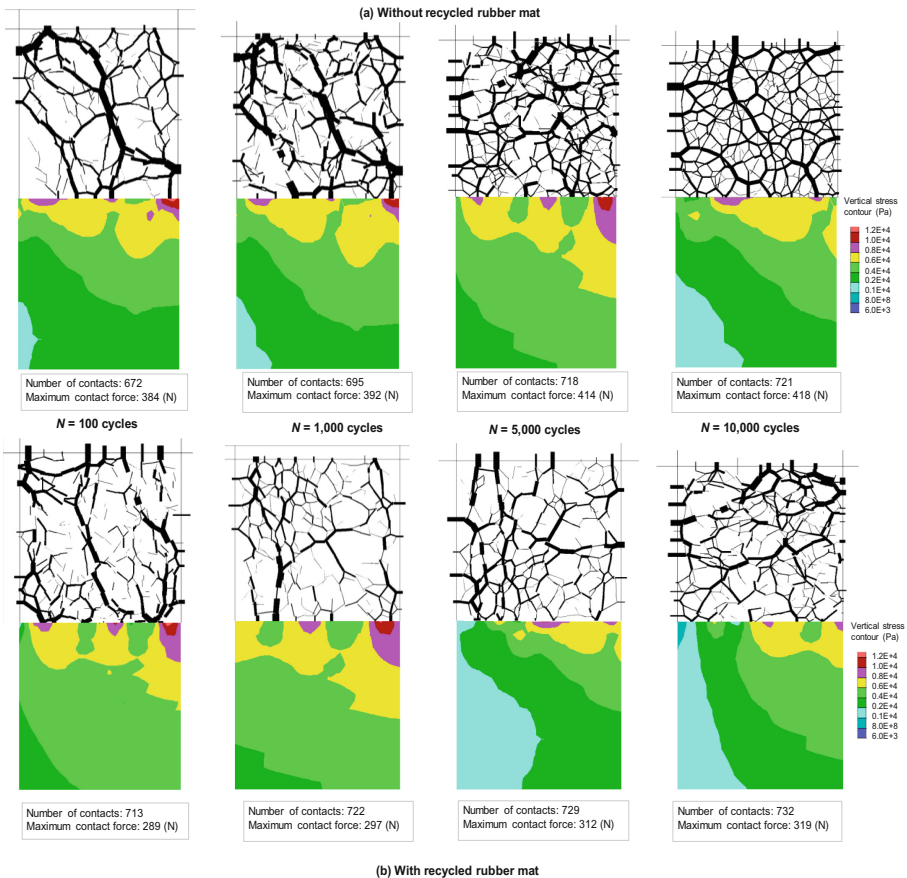


Fig. 5. Distributions of contact forces in ballast layer and vertical stresses predicted for capping and subgrade: (a) without rubber mat; and (b) with a rubber mat (*adopted from Indraratna et al. 2020*).

is clearly seen that the inclusion of rubber mat could increase the contact areas among ballast particles and underneath layers, widen the distribution of vertical stresses; and this in turn decrease magnitude of contact forces the interfaces. Predicted vertical stress at the capping is large at the interfaces with the ballast grains, whereby it is predicted to significantly decrease with depth. An increased applied load cycle N , leads to an increased number of contact force and increased contact force magnitude. This could be associated with the densification and re-arrangement of particles.

4 Conclusions

The following findings can be established:

- Measured laboratory test data proved that the axial deformation, ε_a increased with an increased N and the higher frequency applied the higher ε_a was measured. Ballast grain showed a large axial strain, ε_a within the first $N = 1000$ cycles, followed by a slight increase in the ε_a at a decreased rate.
- The inclusion of a recycled rubber mat resulted in decreased axial strain and breakage of ballast. This was because the mat absorbed cyclic and impact loads and thereby reduced particle breakage of up to 30.8% and 35.3% when subjected to $f = 10, 20\text{Hz}$.
- A coupled DEM-FEM model was introduced to investigate the applied cyclic load-deformation responses of ballast, where discrete grains were modelled by the DEM and the continuum media (REAM, capping and subgrade) were modelled by a continuum media. From the coupled discrete-continuum model (coupled DEM-FEM), the predicted amount of broken bonds (i.e., mimicking particle breakage) increased with increased frequency ($f = 10\text{--}40\text{ Hz}$) and it decreased with the inclusion of a rubber mat.
- The force distributions were studied, and they showed that the forces distributed non-uniformly across the ballast specimens and the inclusion of a rubber mat decreased the magnitude of contact forces which also implied for a reduced particle breakage.

Acknowledgements. The authors acknowledge funding provided by the Australian Government through the ITTC-Rail, (IC170100006). The authors are grateful to the support from organizations including RM CRC and Australasian Centre for Rail Innovation (ACRI) through Project R2.5.1.

References

1. Raymond, G.P., Davies, J.R.: Triaxial tests on dolomite railroad ballast. J. Geotech. Eng. Div. Proc. Am. Soc. Civil Eng. **104**(GT6), 737–751 (1978)
2. Ravitharan, S.S.S., Martin, M.A., Minness, C.: Understanding load transfer characteristics within track sub-structure: queensland experience. In: Conference on Railway Engineering Proceedings: Engineering Innovation for Competitive Edge, Queensland (1998)
3. Sun, Q., Indraratna, B., Ngo, N.T.: Effect of increase in load and frequency on the resilience of railway ballast. Géotechnique **69**(9), 833–840 (2019)

4. Leng, W., Xiao, Y., Nie, R., Zhou, W., Liu, W.: Investigating strength and deformation characteristics of heavy-haul railway embankment materials using large-scale undrained cyclic triaxial tests. *Int. J. Geomech.* **17**(9), 04017074 (2017)
5. Suiker, A.S.J., Borst, R.: A numerical model for the cyclic deterioration of railway tracks. *Int. J. Numer. Meth. Eng.* **57**, 441–470 (2003)
6. Indraratna, B., Ngo, N.T., Rujikiatkamjorn, C.: Deformation of coal fouled ballast stabilized with geogrid under cyclic load. *J. Geotech. Geoenviron. Eng.* **139**(8), 1275–1289 (2013)
7. Jayasuriya, C., Indraratna, B., Ngo, T.: Experimental study to examine the role of under sleeper pads for improved performance of ballast under cyclic loading. *Transp. Geotech.* **19**, 61–73 (2019)
8. Xiao, Y., et al.: Effects of load duration and stress level on deformation and particle breakage of carbonate sands. *Int. J. Geomech.* **20**(7), 06020014 (2020)
9. Xiao, Y., Liu, H., Chen, Y., Jiang, J.: Strength and deformation of rockfill material based on large-scale triaxial compression tests. I: influences of density and pressure. *J. Geotech. Geoenviron. Eng.* **140**(12), 04014070 (2014)
10. Ueng, T.-S., Chen, T.-J.: Energy aspects of particle breakage in drained shear of sands. *Géotechnique* **50**(1), 65–72 (2000)
11. Indraratna, B., Ngo, T.: *Ballast Railroad Design: Smart-Uow Approach*. CRC Press, Boca Raton (2018)
12. Zhai, W.M., Wang, K.Y., Lin, L.H.: Modelling and experiment of railway ballast vibrations. *J. Sound Vib.* **270**, 673–683 (2004)
13. Powrie, W., Yang, L.A., Clayton, C.R.I.: Stress changes in the ground below ballasted railway track during train passage. *Proc. Inst. Mech. Eng. Part F: J. Rail Rapid Transit* 247–261 (2007)
14. McDowell, G.R., Lim, W.L., Collop, A.C., Armitage, R., Thom, N.H.: Comparison of ballast index tests for railway trackbeds. *Geotech. Eng.* **157**(3), 151–161 (2008)
15. Tutumluer, E., Huang, H., Bian, X.: Geogrid-aggregate interlock mechanism investigated through aggregate imaging-based discrete element modeling approach. *Int. J. Geomech.* **12**(4), 391–398 (2012)
16. Ngo, N.T., Indraratna, B., Rujikiatkamjorn, C.: DEM simulation of the behaviour of geogrid stabilised ballast fouled with coal. *Comput. Geotech.* **55**, 224–231 (2014)
17. Leng, J., Gabr, M.A.: Deformation-resistance model for geogrid-reinforced. *Transp. Res. Rec.* **1975**, 146–154 (2006)
18. Navaratnarajah, S.K., Indraratna, B., Ngo, N.T.: Influence of under sleeper pads on ballast behavior under cyclic loading: experimental and numerical studies. *J. Geotech. Geoenviron. Eng.* **144**(9), 04018068 (2018)
19. Priest, J.A., Powrie, W., Yang, L., Grabe, P.J., Clayton, C.R.I.: Measurements of transient ground movements below a ballasted railway line. *Geotechnique* **60**(9), 667–677 (2010)
20. Indraratna, B., Nimbalkar, S.S., Ngo, N.T., Neville, T.: Performance improvement of rail track substructure using artificial inclusions – experimental and numerical studies. *Transp. Geotech.* (2016). <https://doi.org/10.1016/j.trgeo.2016.04.001>
21. 2758.7, A Aggregates and rock for engineering purposes, Part 7. *Railway Ballast*. Standard Australia, 2015. NSW, Australia (2015)
22. Indraratna, B., Ngo, T., Rujikiatkamjorn, C.: Performance of ballast influenced by deformation and degradation: laboratory testing and numerical modeling. *Int. J. Geomech.* **20**(1), 04019138 (2020)
23. McDowell, G.R., Li, H.: Discrete element modelling of scaled railway ballast under triaxial conditions. *Granular Matter* **18**(3), 1 (2016). <https://doi.org/10.1007/s10035-016-0663-8>
24. O’Sullivan, C., Cui, L., O’Neill, C.: Discrete element analysis of the response of granular materials during cyclic loading. *Soils Found.* **48**(4), 511–530 (2008)
25. Aursudkij, B., McDowell, G.R., Collop, A.C.: Cyclic loading of railway ballast under triaxial conditions and in a railway test facility. *Granular Matter* **11**, 391–401 (2009)

26. Huang, H., Tutumluer, E., Hashash, Y.M.A., Ghaboussi, J.: Discrete element modeling of coal dust fouled railroad ballast behavior. In: The 89th Annual Meeting DVD of the Transportation Research Board, Washington, D.C. (2010)
27. Jiang, H., Bian, X., Cheng, C., Chen, Y., Chen, R.: Simulating train moving loads in physical model testing of railway infrastructure and its numerical calibration. *Acta Geotech.* **11**(2), 231–242 (2014). <https://doi.org/10.1007/s11440-014-0327-y>
28. Ngo, N.T., Indraratna, B., Rujikiatkamjorn, C.: A study of the geogrid-subballast interface via experimental evaluation and discrete element modelling. *Granular Matter* **19**(3), 1–16 (2017)